Pattern formation in convection of rotating fluids with broken vertical symmetry

Juan Millán Rodríguez
Departamento de Física y Matemática Aplicada, Facultad de Ciencias, Universidad de Navarra, 31080 Pamplona, Navarra, Spain

Carlos Pérez-García
Departamento de Física y Matemática Aplicada, Facultad de Ciencias, Universidad de Navarra, 31080 Pamplona, Navarra, Spain and Departamento de Física, Universitat Autónoma de Barcelona, 08193 Bellaterra, Catalonia, Spain

Michael Bestehorn, Marc Fantz, and Rudolf Friedrich
Institut für Theorestische Physik und Synergetik der Universität Stuttgart, Pfaffenwaldring 57/4, 7000 Stuttgart 80, Germany
(Received 23 March 1992)

Convective patterns in laterally extended rotating cells with a vertically broken symmetry are analyzed. A simplified model allows one to determine the stability of different basic patterns. By means of a generalized Swift-Hohenberg equation one can study the pattern evolution for different rotation rates and different values of the symmetry-breaking term. In particular, a hexagonal pattern with oscillating amplitudes is analyzed and the role of the defects is discussed.

PACS number(s): 47.25.Qv, 47.20.−k, 47.30.+s

I. INTRODUCTION

Theory and experiments on the Rayleigh-Bénard (RB) instability show that above a critical threshold, plane forms with different symmetries (rolls, squares, hexagons, . . .) can emerge [1–3]. Under rotation around the vertical axis, a convective layer can suffer different instabilities due to the combination of thermal buoyancy, Coriolis, and centrifugal force [4]. For the rotational velocities considered in the present work, centrifugal forces do not play an important role. In this case the instability is ruled by two dimensionless parameters: the Rayleigh (R) number, proportional to the temperature difference ΔT across the fluid layer, and the Taylor number (Ta), proportional to the rotation rate Ω of the container [5]. A particularly surprising nonlinear instability was predicted by Küppers and Lortz [6,7]. They showed that convective rolls lose their stability when a critical rotation rate Ω_c (Ta_c) is reached. The initial rolls are replaced by rolls at $\sim 58°$ in a periodic fashion. Recent experiments confirmed this transition [8,9].

The method of amplitude equations provides a useful framework to study slowly spatial and temporal variations of convective systems [10]. The amplitude equations can be derived from the hydrodynamical equations under suitable approximations. Busse and Heikes [8] used a model based on a system of amplitude equations used before for three competing biological species [11]. This takes advantage of the fact that the rolls rotate almost 60°, and therefore they can be described mainly by three amplitudes. This model shows some similarities with the rotating convective problem. Soward [12] extended these studies taking into account terms that break the vertical symmetry as found in some convective problems. [For example, when the boundary conditions are different on the bottom ($z=0$) and on the top ($z=1$) of the layer or when some parameters (viscosity, thermal expansion, thermal diffusivity) in balance equations depend on temperature.] In these cases the solution of the linear problem is no more symmetric with respect to the midplane. More recently, Goldstein, Knobloch, and Silber [13] studied the normal forms of this problem using the theory of equivariant bifurcations.

This procedure assumes some approximations: it considers that convective patterns in the system have a global preferred direction. But this is difficult to obtain because patterns obtained in experiments achieve a complex dynamics (defects, grain boundaries, . . .). To avoid some of the limitations of the amplitude method, Swift and Hohenberg proposed a model in which the description is made in terms of a spatially fast-varying order parameter [14]. This model is still much simpler for both analytical and numerical work than the full fluid equations. It also has some advantages over the amplitude method, because the Swift-Hohenberg (SH) equation is rotationally invariant and no preferred orientations of convective cells are assumed *a priori*. However, the main disadvantage is that the calculation of coefficients involves some approximations and, therefore, comparison between numerical integrations of this equation and experiments is not easy [15].

In a recent paper a generalized Swift-Hohenberg equation (GSHE) that includes rotation was derived [16]. The corresponding equation predicts that, at small rotation rate (well below Ω_c), and due to the presence of defects, a stable pattern of rolls turns rigidly in the direction of the container rotation. When the rotation is increased further, defects propagate along the sidewall. At the critical

Ta_c the Küppers-Lortz (KL) instability is obtained and the simulations show patterns similar to that observed in experiments. The main aim of the present work is to consider a GSHE including also a term that breaks the vertical symmetry and that may favor a hexagonal structure. This can happen when non-Boussinesq effects are taken into account [17], or if a temperature-dependent surface tension takes place [Bénard-Marangoni (BM) convection] [2,3,18].

The present paper is organized as follow. In Sec. II we carry out the stability analysis of a model based on the three amplitude equations for a rotating convective cell with a hexagonal symmetry [12,19]. In Sec. III, a GSHE is proposed to study the pattern formation. The relationship between the coefficients in the amplitude equations and those in the GSHE is also derived. Simulations of the GSHE [20,21] show that different textures are possible for different values of the rotation rate and of the quadratic term. The role of the defects in the formation and temporal behavior of these textures is discussed.

II. NONLINEAR ANALYSIS: AMPLITUDE EQUATIONS

A. Amplitude equations

A fluid layer with an infinite horizontal extension, heated from below and rotated around a vertical axis, is considered. The hydrodynamical equations that describe this system are well known and their linear stability thresholds were studied many years ago [5]. Nonlinear studies showed the possibility of some primary instabilities (transition from a conductive state to a convective one) and secondary ones (Küppers-Lortz instability). To obtain a better understanding of these phenomena, a simplified model has been proposed [8,12]. In this model only three modes with a wavelength $|k|=k_c$ (the critical one) oriented among them by an angle of $2\pi/3$ (hexagonal lattice) are considered.

The amplitudes are then introduced by projecting the perturbation vector $\Phi=(u,v,w,\theta)$ of the velocity components (u,v,w) and temperature (θ) from the thermally conducting state on three linear unstable modes forming a hexagonal lattice [22]:

$$\Phi(\mathbf{r},t)=[A_1(t)\cos\mathbf{k}_1\cdot\mathbf{x}+A_2(t)\cos\mathbf{k}_2\cdot\mathbf{x}+A_3(t)\cos\mathbf{k}_3\cdot\mathbf{x}]\mathbf{g}(z)+\Phi_s[A_i^2] \quad (1)$$

with $\mathbf{x}=(x,y)$, $\mathbf{k}_1+\mathbf{k}_2+\mathbf{k}_3=0$, and where $\mathbf{g}(z)$ is a function that is obtained from the basic linear equation and boundary conditions [23]. Substitution of (1) into the hydrodynamic equations for a fluid with an infinite Prandtl number ($\mathrm{Pr}=\infty$) leads, after elimination of the linearly stable, enslaved modes Φ_s [24], to a system of coupled nonlinear rate equations for A_i. Taking the nonlinearities up to third order one gets

$$\dot{A}_i=\epsilon A_i+\delta' A_{i+1}A_{i+2}-A_i[A_i^2+(2+\gamma)A_{i+1}^2+(2-\gamma)A_{i+2}^2],\quad i=1,2,3 \bmod(3).$$

Here $\epsilon=(R-R_c)/R_c$, where R_c is the critical value of R for convection to appear. Rescaling with $A_i\equiv A_i/\sqrt{\epsilon}$ we obtain the simplified amplitude equations

$$\dot{A}_i=A_i+\delta A_{i+1}A_{i+2}-A_i[A_i^2+(2+\gamma)A_{i+1}^2+(2-\gamma)A_{i+2}^2],\quad i=1,2,3 \bmod(3), \quad (2)$$

where $\delta=\delta'/\sqrt{\epsilon}$. The coefficient δ reflects the effects that break the vertical symmetry and leads to the possibility of hexagons. The cubic terms usual in convection are modified by a coefficient γ proportional to Ta that accounts for rotation. When rotation is dropped out ($\gamma=0$) the amplitude equations (2) reduce to that proposed in [3] when $A_3=A_1$. For the sake of simplicity spatial variations of A_i are not included. The region of stability for rolls and hexagons can be determined straightforwardly by a linear stability analysis [12].

B. Stability diagram

We briefly summarize the main results on the stability of solutions. Figure 1 gives a sketch of the stability diagram in the space of parameters, ϵ, δ', and γ while Fig. 2 represents a section δ-γ for the same equation rescaled. Even for the simplified model (2) different solutions may be obtained by changing δ and γ. The main regions of stability in Fig. 2 are described in the following.

In region I, rolls are stable. Region II shows hysteresis between rolls and a limit cycle, corresponding to an oscillation of A_i with fixed relative phases. In this region, a third type of solution corresponding to saddle points ($A_i\neq A_{i+1}\neq A_{i+2}\neq 0$) is also possible. In the following we shall refer to these as unstable asymmetric solutions. In region IV, hexagons ($A_i=A_{i+1}=A_{i+2}\neq 0$) are stable, while in region V both stationary rolls and hexagons are stable and a hysteresis between these two solutions can be

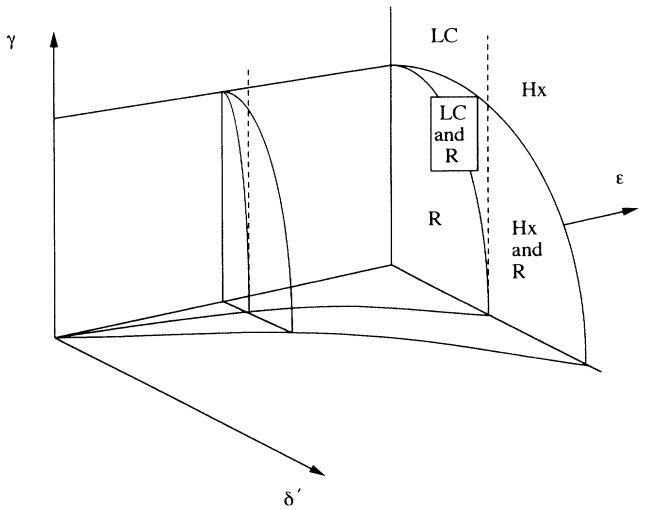

FIG. 1. Stability regions for the different solutions [rolls (R), hexagons (Hx), limit cycle (LC) and hysteresis] in the parameter space $(\delta',\gamma,\epsilon)$ of the 3-mode model [Eq. (1)].

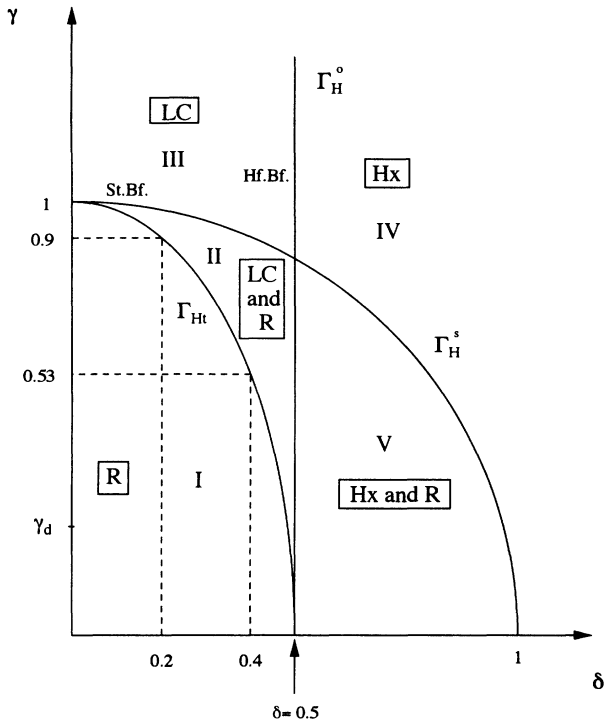

FIG. 2. Stability regions in a δ-γ section for Eq. (2). The Hopf and stationary bifurcations are discussed in the text.

obtained. Starting from hexagons in IV and decreasing δ, a Hopf bifurcation at the line $\Gamma_H^o(\delta=\delta_H^o)$ leads to a stable limit cycle around the hexagonal solution. (However, the rolls continue to be stable when crossing from region V to region II through Γ_H^o.)

Now the relationship of this limit cycle with other solutions in the different regions in the stability diagram (Fig. 2) is described. In region II, the limit cycle grows and approaches the three unstable asymmetric solutions [Figs. 3(c) and 4(a)] when δ decreases. For values of δ on the line Γ_{Ht} the limit cycle meets the asymmetric points and forms a heteroclinic orbit. For values of γ below this Γ_{Ht} curve, the limit cycle becomes unstable with respect to stable rolls. For values of γ above Γ_{Ht} [Fig. 4(a)] that heteroclinic orbit disappears and the limit cycle is always stable [Fig. 4(b)] in regions II and III. The asymmetric points tend to the A_i axis by increasing γ, and for a sufficiently high γ (on the line Γ_R^s) they meet exactly the roll solutions [Fig. 4(c)]. In region III, the limit cycle is the only stable solution. For $\delta=0$, it degenerates into the heteroclinic loop joining the three fixed points on the axis, recovering the KL instability.

III. THE GENERALIZED SWIFT-HOHENBERG EQUATION

In the preceding section, spatial dependence of the amplitudes was not considered. So the corresponding pattern is perfect without dislocations or grain boundaries. Some recent experiments [4,27] have shown that defects and grain boundaries play a crucial role in the dynamics of rotating convective patterns. The main processes observed cannot be explained simply by the global dynamics of three unstable fixed points or a limit cycle as in the preceding section, but spatial terms responsible for the defects must be included.

We then propose a generalized SH model that includes spatial variations in a coherent manner. For the sake of simplicity we restrict the analysis for $Pr=\infty$, fluids although this condition is almost fulfilled for $Pr \geq 5$. (However, comparison with the experiments in [9,27] done for $Pr \leq 1$ will require two order-parameter equations [25].)

A. Formulation

Starting with the hydrodynamic equations in the Boussinesq approximation for a rotating Rayleigh-Bénard instability [5] in a liquid with a high Pr value, a minimal GSHE may be derived that describes the dynamics and

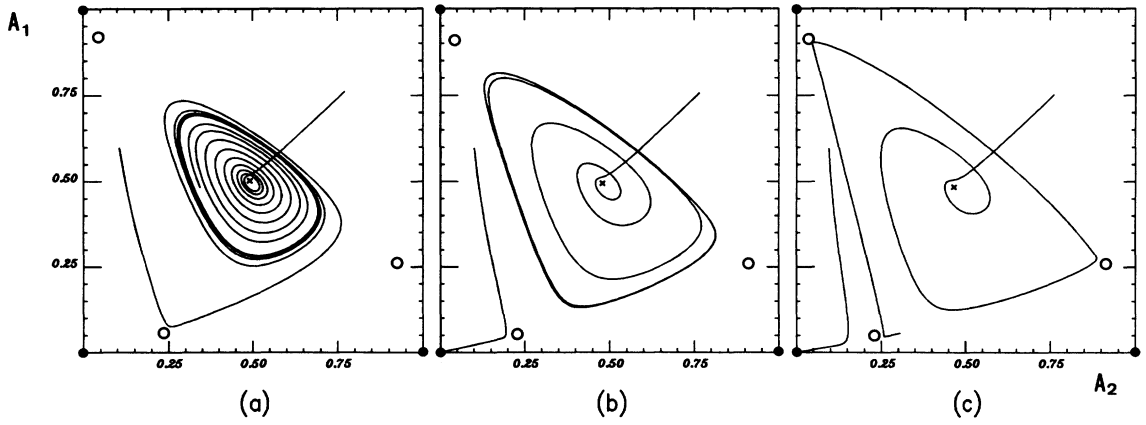

FIG. 3. Solution of the amplitude equations in the A_1-A_2 plane for fixed $\gamma=0.81$ and decreasing values of δ corresponding to different stability regions in Fig. 2: (a) $\delta=0.456$ (region II), (b) $\delta=0.365$ (region II), (c) $\delta=0.27$ (line Γ_{Ht}). The limit cycle around the hexagon solution is growing [(a),(b)] until a heteroclinic orbit appears [(c)] due to the collision between the limit cycle and the saddle points near the roll solutions. (●, roll solution; ○, asymmetric solution; ×, hexagonal solution.)

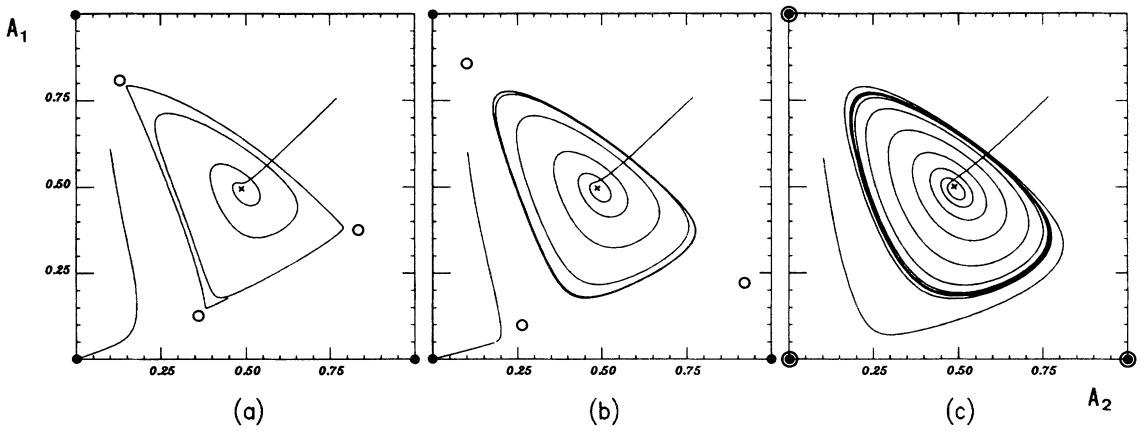

FIG. 4. Temporal evolution of amplitude equations projected in the A_1-A_2 plane. For fixed $\delta=0.4$ three different solutions are obtained: (a) a heteroclinic orbit between three different points near the solutions of rolls at line $\Gamma_{\rm Ht}$ ($\gamma=0.53$); (b) a limit cycle and stationary rolls in the region II ($\gamma=0.75$) (notice that three saddle points approach the roll solutions); (c) the roll solutions become unstable in region III ($\gamma=1.1$). (●, roll solution; ○, asymmetric solution; ×, hexagonal solution.)

evolution of patterns in large aspect ratio cells [16]. In that paper it is demonstrated that for rotation to be described, at least one new term in the usual SHE must be included. This is a cubic term that also involves spatial derivatives. Here we further generalize this equation including vertical symmetry-breaking effects. To study the situations similar to that discussed in the preceding section for the amplitude equations, we investigate the following GSH equation:

$$\dot{\Psi}(\mathbf{x},t)=[\epsilon-(1+\Delta)^2]\Psi(\mathbf{x},t)+\tilde{\delta}\Psi^2(\mathbf{x},t) -\Psi^3(\mathbf{x},t)-\tilde{\gamma}[\nabla\Psi(\mathbf{x},t)\times\nabla\Delta\Psi^2(\mathbf{x},t)]_z \quad (3)$$

where Ψ is proportional to the deviations of the temperature with respect to the conductive state, Δ and ∇ are the two-dimensional (2D) Laplacian and the 2D gradient, respectively. This may be considered as the minimal model that includes the main features found in Sec. II B. For the sake of simplicity, we include neither terms of the same nor of higher order in the spatial derivatives.

A more important difference between Eq. (3) and the usual SHE is that the term due to the rotation is nonvariational, i.e., Eq. (3) cannot be derived from a potential. The rotation breaks the reflection symmetry ($x\rightarrow -x$ or $y\rightarrow -y$) and precludes the existence of a potential that decreases monotonically towards a stationary state. If $\tilde{\delta}=0$ one recovers the GSHE discussed by Fantz *et al.* [16]. The quadratic term in this equation is responsible for the breaking of the vertical symmetry of the linear solution [17,24]. In the limit $\tilde{\delta}=\tilde{\gamma}=0$, Eq. (3) reduces to the well-known SH equation [14,15,20] that leads to a pattern of rolls while for $\tilde{\delta}\neq 0, \tilde{\gamma}=0$ (no rotation) stationary hexagonal patterns can also be obtained [20].

B. Numerical solutions in cylindrical containers

The simulation of Eq. (3) was made for the usual lateral boundary conditions $\Psi=\partial_n\Psi=0$ (where n denotes the direction perpendicular to the sidewalls) that corresponds to vanishing velocity components on the thermal insulating sidewalls. In order to solve the GSHE we use a semi-implicit pseudospectral method described elsewhere [26]. The nonlinearities are calculated in real space and the spatial derivatives are evaluated by finite differences.

The coefficients of the amplitude equations (2) and the GSHE (3) can be simply related by assuming $\Psi=\sum_{i=1}^{3} A_i \exp(i\mathbf{kr})+\text{c.c.}$, where c.c. stands for the complex-conjugated term. This identification leads to

$$\delta=\frac{2\tilde{\delta}}{\sqrt{3\epsilon}}, \quad \gamma=\frac{2\tilde{\gamma}}{\sqrt{3}} . \quad (4)$$

These relationships allow us to compare results in Eq. (3) for values in the stability regions described in Sec. II B, i.e., to interpret the patterns obtained by numerical simulations of Eq. (3) in terms of the different solutions in Fig. 2. But the main point now is that the GSHE includes the spatial variations and also finite containers can give a clearer idea of the pattern that could be observed in real experiments. The patterns are integrated on a cylindrical cell as used in experiments.

1. Rigid rotation of the pattern

We assume parameter values in region I where rolls are the stable solution of Eq. (2). Starting from a random initial condition, simulations of the GSHE (3) give patterns with parallel rolls in the central part and some defects localized on two opposite zones on the walls. Below a rotation rate corresponding to a value for $\gamma=\gamma_d$ (that depends on the aspect ratio), the defects tend to travel by the lateral wall, forcing the rolls to bend and rotate, as obtained by Fantz *et al.* [16]. Above γ_d defects are radiated from one region of defects to the other. This last feature has been observed in recent experiments by Zhong, Ecke, and Steinberg [4] at a rotation rate below the KL instability.

Patterns of hexagons are obtained for parameters in regions III and IV. A rigid rotation of the whole pattern is observed (Fig. 5). This rotation velocity is related to the

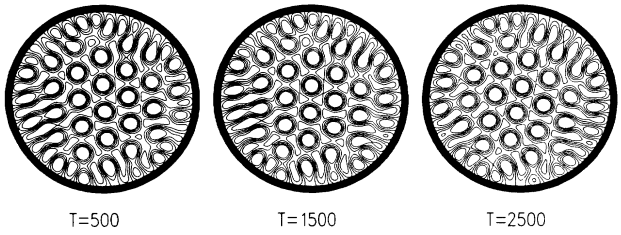

FIG. 5. Solution of the GSHE showing a rigid rotation of a hexagonal pattern ($\delta=0.657, \gamma=1.1, \epsilon=0.1$).

defects present in the pattern and the nonvariational term in Eq. (3) [16]. Numerical results show that hexagons have a rigid rotation velocity lower than a pattern of rolls, probably due to the fact that the former fill a cylindrical geometry better than the latter.

2. *Küppers-Lortz-like instability*

Rolls and a limit cycle are stable in region II of Fig. 2. The limit-cycle solution resembles the heteroclinic connection among the three asymmetric solutions. The later points are near but do not coincide with the roll solutions of the KL transition. However, as these solutions do not differ so much, they ought to lead to similar patterns in the simulations. This is why we designed this case generically as KL-like instability.

In simulations, only the limit-cycle solution is obtained because some defects are always present. This fact precludes a solution of rolls with a fixed orientation. Then we observe in the simulations a continuous transition between rolls at 60° not predicted by the KL instability. In fact the last one assumes that a system of rolls reaches a finite amplitude, then becomes unstable, and a new set of rolls grows with a wave vector rotated an angle α relative to the first set. However, the mechanism observed in simulations of the GSH model is qualitatively different. The mechanism of the pattern reorientation is shown in Fig. 6. Defects near the walls are oriented at some angle with respect to the central region. These regions of defects grow towards the center and erode the central rolls along the direction of the defects leading to a reorientation, similar to that observed in experiments in high aspect ratio cells [4]. The growth process of defects is enhanced by the breaking of bended rolls on several grain boundaries that propagate at a fixed angle in the azimuthal direction. This transition is similar to that observed in [27], in spite of the difference in Pr value between the present simulations and that experiment. For some values a single grain boundary is observed that does not induce sudden orientation change but increases the rotation velocity of the whole pattern (Fig. 7).

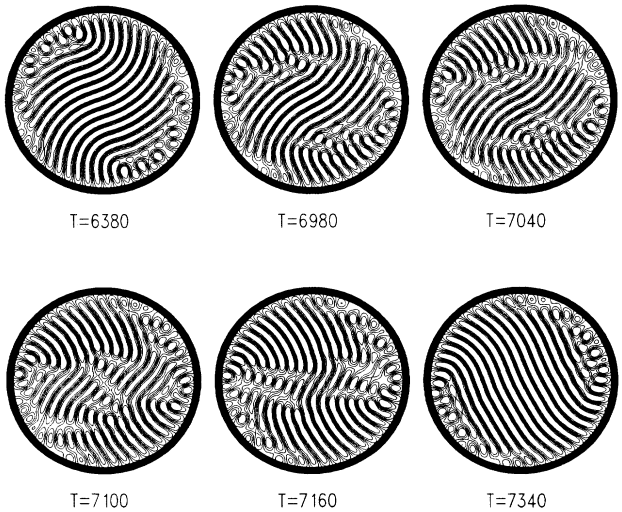

FIG. 6. Solution of Eq. (3) for $\delta=0.2$, $\gamma=0.9$, and $\epsilon=0.1$. The growth and propagation of defects at $\sim 60°$ erode the pattern of rolls in the center of the cell. Grain boundaries travel across the bended rolls and break them, generating another direction that replaces the previous one.

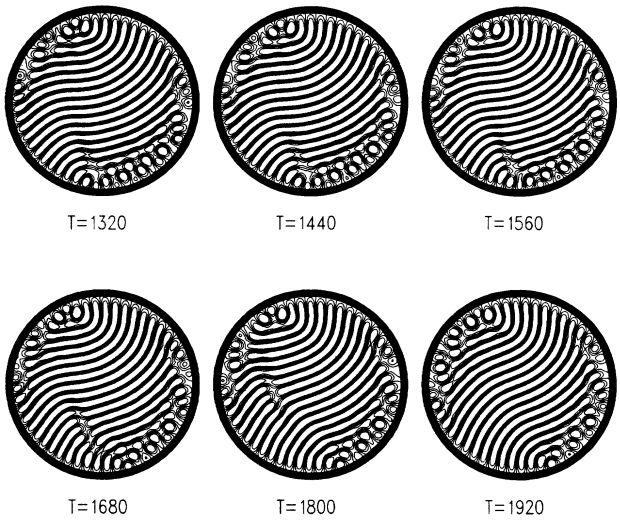

FIG. 7. Solitary grain boundary traveling across the texture produces a sudden increment in the rotation of the pattern.

Nevertheless, when we integrate Eq. (3) for periodic boundary conditions (which mimic an infinite system), the temporal evolution leads to a pattern of fixed rolls for the wide parameter region studied numerically. These features suggest that the lateral walls and the defects play an important role in the evolution of textures.

3. *Three-mode limit cycle*

We are interested in this case in simulations on small Γ cells, because this allows one to consider the important role of defects discussed above. In this case our aim is to visualize what kind of patterns correspond to a limit cycle in the stability diagram (Fig. 2). Figure 8 shows solutions of Eq. (3) corresponding to a point ($\delta=0.4, \gamma=1.1$) of region III in Fig. 2. In this situation the amplitude equations show that the limit cycle surrounds the hexagonal solution and it is far from the KL instability. Then the three amplitudes must change cyclically in a continuous way.

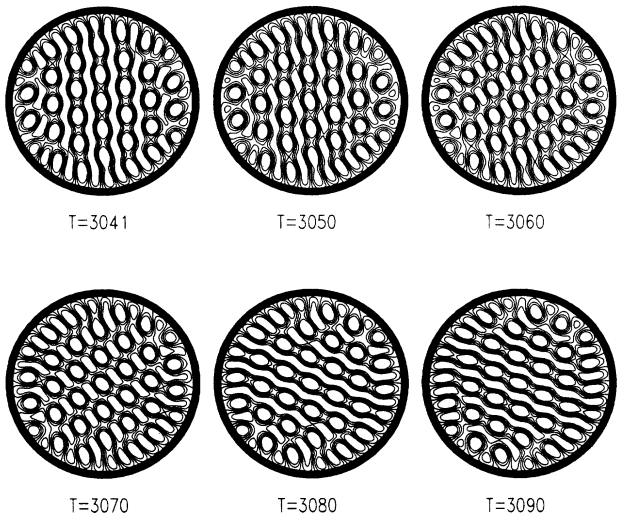

FIG. 8. Limit cycle ($\delta=0.4$, $\gamma=1.1$) in a circular container. The system passes near the three asymmetric solutions in a periodic sequence.

In the first pattern in Fig. 8, one of three hexagonal modes is dominant. During the evolution some states are observed where two modes give rise to a nearly rhomboid lattice while the amplitude of the third mode is very small. After some time a new orientation becomes dominant (see last pattern in Fig. 8). The hexagonal form remains, but with a global change of amplitudes in the whole pattern.

IV. CONCLUSIONS

By means of a model of amplitude equations we investigate convection in a horizontal rotating fluid layer with some effect that breaks the vertical symmetry (BM convection, non-Boussinesq effects, etc.).

Numerical results on this model show that the hexagons may lose their stability via a Hopf bifurcation. The evolution of the corresponding limit cycle in the parameter space is described in some detail. The rolls lose their stability through a stationary bifurcation. Below this line it is possible to find a pattern evolution similar to that in the Küppers-Lortz instability. The difference is that in the present case the limit cycle passes near three asymmetric solutions but it does not coincide with the heteroclinic orbit connecting three exact roll solutions.

The amplitude model does not provide a complete study of the possible textures in a real system because it is restricted to three modes and includes neither spatial terms nor the lateral boundaries. However, the stability analysis of these equations gives important insight to determine the most important mechanisms that one may encounter by posterior integration of the GSH model. The last one includes lateral walls and spatial effects giving more complete information on the patterns to be observed. For example GSHE predicts a rigid rotation of a hexagonal pattern in small aspect ratio. (This prediction could be easily checked under suitable experimental conditions.) Another interesting feature of solutions of the GSH model is the role that the defects seem to play (always present in finite geometries) in the KL-like mechanisms. For a rotating hexagonal pattern global continuous change in the modes is observed (Fig. 8). This is in agreement with the limit-cycle solution in the amplitude model. The numerical solutions of the GSH model have qualitative agreement with some features observed in recent experiments [4,27]. The present model also suggests that it could be interesting to derive an amplitude model that would include spatial derivatives, in order to obtain the dynamic of defects and grain boundaries in rotating convective cells.

ACKNOWLEDGMENTS

This work has been partially supported by an EEC grant SC311 (M.B.) and the DGICYT (Spanish Government) grant PB90-0362 (J.M. and C.P-G.). We also appreciate financial support from a Spanish-German Integrated Action (No. 26, 1991; No. 73, 1992).

[1] *Cellular Structures in Instabilities*, edited by J. E. Wesfired and S. Zaleski (Springer, Berlin, 1984).
[2] E. Palm, J. Fluid Mech. **8**, 183 (1960).
[3] L. A. Segel and J. T. Stuart, J. Fluid Mech. **13**, 289 (1962).
[4] F. Zhong, R. Ecke, and V. Steinberg, Physica D **51**, 596 (1991).
[5] S. Chandrasekhar, *Hydrodynamic and Hydromagnetic Stability* (Clarendon, Oxford, 1961).
[6] G. Küppers and D. Lortz, J. Fluid Mech. **35**, 609 (1969); G. Küppers, Phys. Lett. **32A**, 7 (1970).
[7] R. M. Clever and F. H. Busse, J. Fluid Mech. **94**, 609 (1979).
[8] K. E. Heikes and F. H. Busse, Ann. (N.Y.) Acad. Sci. **357**, 28 (1980)
[9] J. J. Niemela and R. J. Donnelly, Phys. Rev. Lett. **57**, 2524 (1988).
[10] A. C. Newell and J. A. Whitehead, J. Fluid Mech. **38**, 279 (1969).
[11] R. M. May and W. J. Leonard, SIAM J. Appl. Math. **29**, 243 (1975).
[12] A. M. Soward, Physica **14D**, 227 (1985).
[13] H. F. Goldstein, E. Knobloch, and M. Silber (unpublished).
[14] J. Swift and P. C. Hohenberg, Phys. Rev. A **15**, 319 (1977).
[15] H. S. Greenside, W. M. Coughran, Jr., and N. L. Schryer, Phys. Rev. Lett. **49**, 726 (1982).
[16] M. Fantz, R. Friedrich, M. Bestehorn, and H. Haken (unpublished).
[17] F. H. Busse, J. Fluid Mech. **30**, 625 (1967); S. Ciliberto, E. Pampaloni, and C. Pérez-García, J. Stat. Phys. **64**, 1045 (1991).
[18] H. Bénard, Rev. Gen. Sci. Rev. Appl. **11**, 1261 (1900).
[19] J. W. Swift, Contemp. Math. **28**, 435 (1984).
[20] M. Bestehorn and H. Haken, Z. Phys. B **57**, 329 (1984).

[21] R. Friedrich, M. Bestehorn, and H. Haken, J. Mod. Phys. B **4**, 365 (1990).
[22] L. A. Segel, J. Fluid Mech. **21**, 345 (1965).
[23] F. H. Busse, Rep. Prog. Phys. **41**, 1929 (1978).
[24] H. Haken, *Synergetics: An Introduction,* 2nd ed. (Springer, Berlin, 1978); *Advanced Synergetics* (Springer, Berlin, 1983).
[25] D. Siggia and A. Zippelius, Phys. Rev. Lett. **47**, 835 (1981).
[26] M. Bestehorn, Ph.D. thesis, Universität Stuttgart (1988).
[27] E. Bodenschatz, D. S. Cannell, J. de Bruyn, R. Ecke, Y. Hu, K. Lerman, and G. Ahlers, Physica D (to be published).

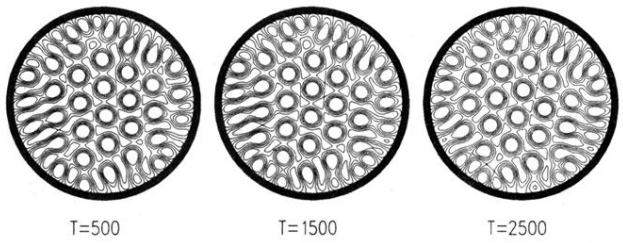

FIG. 5. Solution of the GSHE showing a rigid rotation of a hexagonal pattern ($\delta=0.657, \gamma=1.1, \epsilon=0.1$).

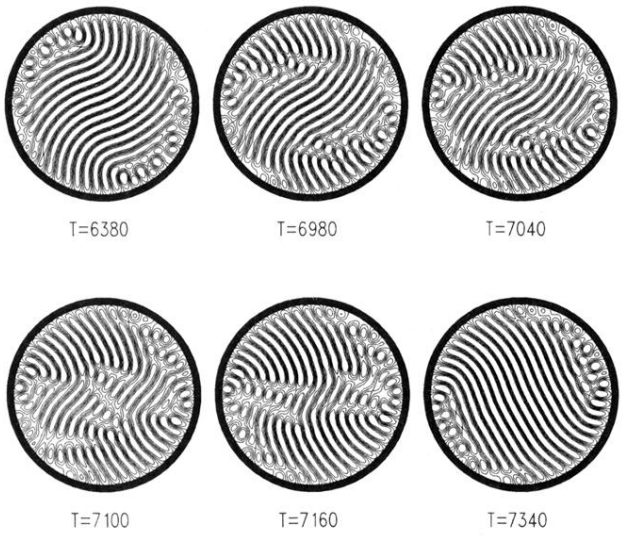

FIG. 6. Solution of Eq. (3) for $\delta=0.2$, $\gamma=0.9$, and $\epsilon=0.1$. The growth and propagation of defects at $\sim 60°$ erode the pattern of rolls in the center of the cell. Grain boundaries travel across the bended rolls and break them, generating another direction that replaces the previous one.

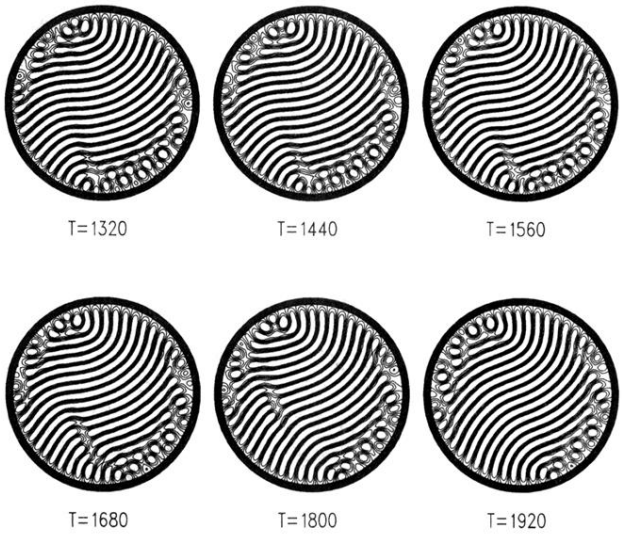

FIG. 7. Solitary grain boundary traveling across the texture produces a sudden increment in the rotation of the pattern.

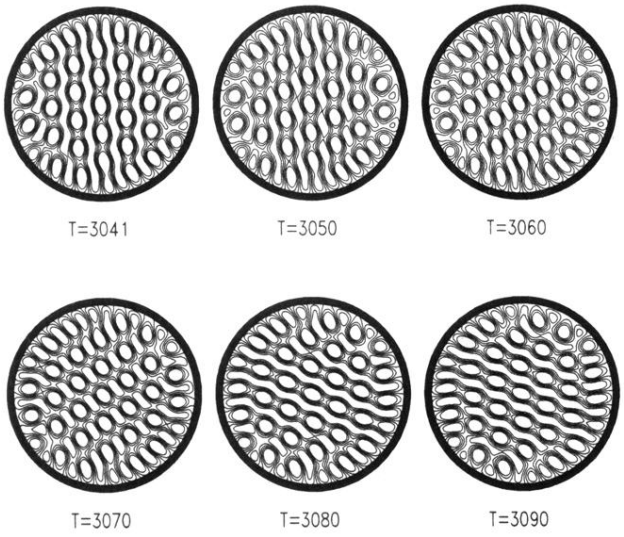

FIG. 8. Limit cycle ($\delta=0.4$, $\gamma=1.1$) in a circular container. The system passes near the three asymmetric solutions in a periodic sequence.